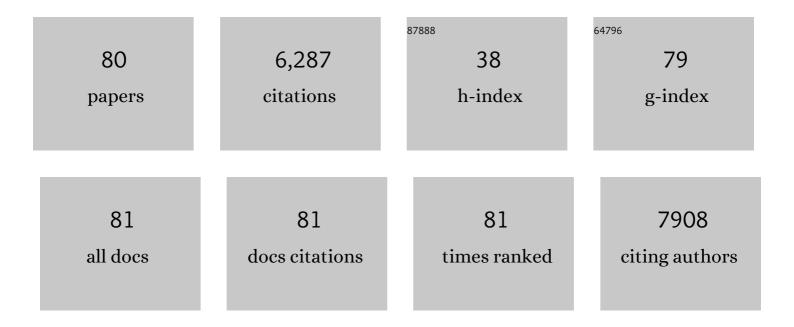
## Guohui Tian

List of Publications by Year in descending order

Source: https://exaly.com/author-pdf/2167089/publications.pdf Version: 2024-02-01



Спонті Тим

#	Article	IF	CITATIONS
1	Molecule Self-Assembly Synthesis of Porous Few-Layer Carbon Nitride for Highly Efficient Photoredox Catalysis. Journal of the American Chemical Society, 2019, 141, 2508-2515.	13.7	685
2	Wellâ€Ordered Largeâ€Pore Mesoporous Anatase TiO <sub>2</sub> with Remarkably High Thermal Stability and Improved Crystallinity: Preparation, Characterization, and Photocatalytic Performance. Advanced Functional Materials, 2011, 21, 1922-1930.	14.9	431
3	Facile solvothermal synthesis of hierarchical flower-like Bi <sub>2</sub> MoO <sub>6</sub> hollow spheres as high performance visible-light driven photocatalysts. Journal of Materials Chemistry, 2011, 21, 887-892.	6.7	427
4	Preparation and Characterization of Stable Biphase TiO <sub>2</sub> Photocatalyst with High Crystallinity, Large Surface Area, and Enhanced Photoactivity. Journal of Physical Chemistry C, 2008, 112, 3083-3089.	3.1	288
5	3D hierarchical flower-like TiO2 nanostructure: morphology control and its photocatalytic property. CrystEngComm, 2011, 13, 2994.	2.6	237
6	Facile strategy for controllable synthesis of stable mesoporous black TiO <sub>2</sub> hollow spheres with efficient solar-driven photocatalytic hydrogen evolution. Journal of Materials Chemistry A, 2016, 4, 7495-7502.	10.3	198
7	NiSeâ€Ni <sub>0.85</sub> Se Heterostructure Nanoflake Arrays on Carbon Paper as Efficient Electrocatalysts for Overall Water Splitting. Small, 2018, 14, e1800763.	10.0	185
8	Hierarchical Core–Shell Carbon Nanofiber@ZnIn <sub>2</sub> S <sub>4</sub> Composites for Enhanced Hydrogen Evolution Performance. ACS Applied Materials & Interfaces, 2014, 6, 13841-13849.	8.0	179
9	Facile preparation of porous NiTiO3 nanorods with enhanced visible-light-driven photocatalytic performance. Journal of Materials Chemistry, 2012, 22, 16471.	6.7	176
10	Cubic quantum dot/hexagonal microsphere Znln <sub>2</sub> S <sub>4</sub> heterophase junctions for exceptional visible-light-driven photocatalytic H <sub>2</sub> evolution. Journal of Materials Chemistry A, 2017, 5, 8451-8460.	10.3	176
11	Synthesis and photocatalytic activity of stable nanocrystalline TiO2 with high crystallinity and large surface area. Journal of Hazardous Materials, 2009, 161, 1122-1130.	12.4	172
12	Facile synthesis of sheet-like ZnO assembly composed of small ZnO particles for highly efficient photocatalysis. Journal of Materials Chemistry A, 2013, 1, 5700.	10.3	170
13	Surface oxygen vacancy defect-promoted electron-hole separation for porous defective ZnO hexagonal plates and enhanced solar-driven photocatalytic performance. Chemical Engineering Journal, 2020, 379, 122295.	12.7	170
14	Carbothermal synthesis of ordered mesoporous carbon-supported nano zero-valent iron with enhanced stability and activity for hexavalent chromium reduction. Journal of Hazardous Materials, 2016, 309, 249-258.	12.4	131
15	Hierarchical composites of TiO2 nanowire arrays on reduced graphene oxide nanosheets with enhanced photocatalytic hydrogen evolution performance. Journal of Materials Chemistry A, 2014, 2, 4366-4374.	10.3	112
16	Growth rate controlled synthesis of hierarchical Bi2S3/In2S3 core/shell microspheres with enhanced photocatalytic activity. Scientific Reports, 2014, 4, 4027.	3.3	108
17	Hierarchical CuS hollow nanospheres and their structure-enhanced visible light photocatalytic properties. CrystEngComm, 2013, 15, 5144.	2.6	106
18	Hierarchical flake-like Bi2MoO6/TiO2 bilayer films for visible-light-induced self-cleaning applications. Journal of Materials Chemistry A, 2013, 1, 6961.	10.3	102

#	Article	IF	CITATIONS
19	Composites of small Ag clusters confined in the channels of well-ordered mesoporous anatase TiO2 and their excellent solar-light-driven photocatalytic performance. Nano Research, 2014, 7, 731-742.	10.4	102
20	Self-floating amphiphilic black TiO2 foams with 3D macro-mesoporous architectures as efficient solar-driven photocatalysts. Applied Catalysis B: Environmental, 2017, 206, 336-343.	20.2	102
21	Enhanced photocatalytic activity of S-doped TiO2–ZrO2 nanoparticles under visible-light irradiation. Journal of Hazardous Materials, 2009, 166, 939-944.	12.4	101
22	Controlled synthesis of thorny anatase TiO <sub>2</sub> tubes for construction of Ag–AgBr/TiO <sub>2</sub> composites as highly efficient simulated solar-light photocatalyst. Journal of Materials Chemistry, 2012, 22, 2081-2088.	6.7	84
23	In situ growth of Bi <sub>2</sub> MoO <sub>6</sub> on reduced graphene oxide nanosheets for improved visible-light photocatalytic activity. CrystEngComm, 2014, 16, 842-849.	2.6	80
24	Assembly of TiO2 ultrathin nanosheets with surface lattice distortion for solar-light-driven photocatalytic hydrogen evolution. Applied Catalysis B: Environmental, 2018, 239, 317-323.	20.2	77
25	Black N/Hâ€TiO <sub>2</sub> Nanoplates with a Flowerâ€Like Hierarchical Architecture for Photocatalytic Hydrogen Evolution. ChemSusChem, 2016, 9, 2841-2848.	6.8	73
26	Controlled synthesis of mesoporous anatase TiO2 microspheres as a scattering layer to enhance the photoelectrical conversion efficiency. Journal of Materials Chemistry A, 2013, 1, 9853.	10.3	70
27	Hierarchical SnS <sub>2</sub> /CuInS <sub>2</sub> Nanosheet Heterostructure Films Decorated with C <sub>60</sub> for Remarkable Photoelectrochemical Water Splitting. ACS Applied Materials & Interfaces, 2019, 11, 9093-9101.	8.0	68
28	Exceptional visible-light photoelectrocatalytic activity of In2O3/In2S3/CdS ternary stereoscopic porous heterostructure film for the degradation of persistent 4-fluoro-3-methylphenol. Applied Catalysis B: Environmental, 2018, 225, 477-486.	20.2	66
29	A Floating Porous Crystalline TiO <sub>2</sub> Ceramic with Enhanced Photocatalytic Performance for Wastewater Decontamination. European Journal of Inorganic Chemistry, 2013, 2013, 2411-2417.	2.0	59
30	Hierarchical Composite of Ag/AgBr Nanoparticles Supported on Bi <sub>2</sub> MoO <sub>6</sub> Hollow Spheres for Enhanced Visibleâ€Light Photocatalytic Performance. ChemPlusChem, 2013, 78, 117-123.	2.8	58
31	Enhanced Photocatalytic Hydrogen Evolution over Hierarchical Composites of ZnIn <sub>2</sub> S <sub>4</sub> Nanosheets Grown on MoS <sub>2</sub> Slices. Chemistry - an Asian Journal, 2014, 9, 1291-1297.	3.3	57
32	In situ formation of a ZnO/ZnSe nanonail array as a photoelectrode for enhanced photoelectrochemical water oxidation performance. Nanoscale, 2016, 8, 9366-9375.	5.6	52
33	Sulfur doped In2O3-CeO2 hollow hexagonal prisms with carbon coating for efficient photocatalytic CO2 reduction. Chemical Engineering Journal, 2021, 421, 129968.	12.7	52
34	Hierarchical FeTiO <sub>3</sub> –TiO <sub>2</sub> hollow spheres for efficient simulated sunlight-driven water oxidation. Nanoscale, 2015, 7, 15924-15934.	5.6	50
35	Fabrication of size-controlled hierarchical ZnS@ZnIn2S4 heterostructured cages for enhanced gas-phase CO2 photoreduction. Journal of Colloid and Interface Science, 2022, 605, 253-262.	9.4	47
36	Hierarchical Cu7S4-Cu9S8 heterostructure hollow cubes for photothermal aerobic oxidation of amines. Chemical Engineering Journal, 2019, 363, 247-258.	12.7	45

#	Article	IF	CITATIONS
37	Enhanced charge transfer and separation of hierarchical hydrogenated TiO <sub>2</sub> nanothorns/carbon nanofibers composites decorated by NiS quantum dots for remarkable photocatalytic H <sub>2</sub> production activity. Nanoscale, 2018, 10, 4041-4050.	5.6	39
38	Highly dispersed of Ni0.85Se nanoparticles on nitrogen-doped graphene oxide as efficient and durable electrocatalyst for hydrogen evolution reaction. Electrochimica Acta, 2018, 262, 107-114.	5.2	39
39	WO3/BiVO4/BiOCl porous nanosheet composites from a biomass template for photocatalytic organic pollutant degradation. Journal of Alloys and Compounds, 2019, 802, 76-85.	5.5	39
40	Surface Plasmon Resonanceâ€Enhanced Visibleâ€NIRâ€Driven Photocatalytic and Photothermal Catalytic Performance by Ag/Mesoporous Black TiO <sub>2</sub> Nanotube Heterojunctions. Chemistry - an Asian Journal, 2019, 14, 177-186.	3.3	39
41	Room temperature solution synthesis of hierarchical bow-like Cu2O with high visible light driven photocatalytic activity. RSC Advances, 2012, 2, 2875.	3.6	38
42	One-step synthesis of a hierarchical Bi <sub>2</sub> S <sub>3</sub> nanoflowerIn <sub>2</sub> S <sub>3</sub> nanosheet composite with efficient visible-light photocatalytic activity. CrystEngComm, 2015, 17, 8720-8727.	2.6	38
43	Hierarchical CuS@ZnIn <sub>2</sub> S <sub>4</sub> Hollow Double-Shelled p–n Heterojunction Octahedra Decorated with Fullerene C <sub>60</sub> for Remarkable Selectivity and Activity of CO <sub>2</sub> Photoreduction into CH <sub>4</sub> . ACS Applied Materials & Interfaces, 2022, 14. 7888-7899.	8.0	34
44	Hydrogenated TiO2/SrTiO3 porous microspheres with tunable band structure for solar-light photocatalytic H2 and O2 evolution. Science China Materials, 2016, 59, 1003-1016.	6.3	32
45	Ultrathin-layered MoS2 hollow nanospheres decorating Ni3S2 nanowires as high effective self-supporting electrode for hydrogen evolution reaction. International Journal of Hydrogen Energy, 2020, 45, 13149-13162.	7.1	31
46	Hierarchical Nâ€Doped TiO <sub>2</sub> Microspheres with Exposed (001) Facets for Enhanced Visible Light Catalysis. European Journal of Inorganic Chemistry, 2014, 2014, 2146-2152.	2.0	29
47	Large-scale synthesis of stable mesoporous black TiO <sub>2</sub> nanosheets for efficient solar-driven photocatalytic hydrogen evolution via an earth-abundant low-cost biotemplate. RSC Advances, 2016, 6, 50506-50512.	3.6	29
48	Hierarchical Co <sub>0.85</sub> Se dSe/MoSe <sub>2</sub> /CdSe Sandwichâ€Like Heterostructured Cages for Efficient Photocatalytic CO <sub>2</sub> Reduction. Small, 2021, 17, e2100412.	10.0	29
49	Hierarchical ZnO nanorod/ZnFe2O4 nanosheet core/shell nanoarray decorated with PbS quantum dots for efficient photoelectrochemical water splitting. Journal of Alloys and Compounds, 2020, 828, 154449.	5.5	28
50	Single-step pyrolytic preparation of Mo2C/graphitic carbon nanocomposite as catalyst carrier for the direct liquid-feed fuel cells. RSC Advances, 2013, 3, 4771.	3.6	27
51	Controlled synthesis and exceptional photoelectrocatalytic properties of Bi2S3/MoS2/Bi2MoO6 ternary hetero-structured porous film. Journal of Colloid and Interface Science, 2019, 555, 214-223.	9.4	26
52	A facile and green synthesis route towards two-dimensional TiO2@Ag heterojunction structure with enhanced visible light photocatalytic activity. CrystEngComm, 2013, 15, 5821.	2.6	25
53	Surface defect-mediated efficient electron-hole separation in hierarchical flower-like bismuth molybdate hollow spheres for enhanced visible-light-driven photocatalytic performance. Journal of Colloid and Interface Science, 2018, 531, 664-671.	9.4	25
54	Hierarchical Ag/Ag <sub>2</sub> S/CuS Ternary Heterostructure Composite as an Efficient Visible‣ight Photocatalyst. ChemCatChem, 2015, 7, 1684-1690.	3.7	23

#	Article	IF	CITATIONS
55	Hydrogenated Cu <sub>2</sub> OAu@CeO <sub>2</sub> Z-scheme catalyst for photocatalytic oxidation of amines to imines. Catalysis Science and Technology, 2018, 8, 5535-5543.	4.1	23
56	Solvothermal Synthesis, Characterization, and Formation Mechanism of a Singleâ€Layer Anatase TiO <sub>2</sub> Nanosheet with a Porous Structure. European Journal of Inorganic Chemistry, 2011, 2011, 754-760.	2.0	22
57	Nickel–Cobalt Diselenide Nanosheets Supported on Copper Nanowire Arrays for Synergistic Electrocatalytic Oxygen Evolution. Advanced Materials Interfaces, 2019, 6, 1802052.	3.7	22
58	Facile Strategy to Fabricate Uniform Black TiO <sub>2</sub> Nanothorns/Graphene/Black TiO <sub>2</sub> Nanothorns Sandwichlike Nanosheets for Excellent Solarâ€Driven Photocatalytic Performance. ChemCatChem, 2016, 8, 3240-3246.	3.7	21
59	Hydrogenated CeO <sub>2â^'x</sub> S <sub>x</sub> mesoporous hollow spheres for enhanced solar driven water oxidation. Chemical Communications, 2016, 52, 2521-2524.	4.1	21
60	Boosted charge transfer and photocatalytic CO2 reduction over sulfur-doped C3N4 porous nanosheets with embedded SnS2-SnO2 nanojunctions. Science China Materials, 2022, 65, 400-412.	6.3	21
61	Tuning in BiVO4/Bi4V2O10 porous heterophase nanospheres for synergistic photocatalytic degradation of organic pollutants. Applied Surface Science, 2019, 470, 631-638.	6.1	20
62	Facile synthesis and shape control of Fe3O4 nanocrystals with good dispersion and stabilization. CrystEngComm, 2013, 15, 3366.	2.6	19
63	Hierarchical NiS decorated CuO@ZnFe2O4 nanoarrays as advanced photocathodes for hydrogen evolution reaction. International Journal of Hydrogen Energy, 2020, 45, 6174-6183.	7.1	19
64	Hierarchical CuCo <sub>2</sub> S <sub>4</sub> Nanoflake Arrays Grown on Carbon Cloth: A Remarkable Bifunctional Electrocatalyst for Overall Water Splitting. ChemElectroChem, 2021, 8, 1134-1140.	3.4	19
65	Homojunction and defect synergy-mediated electron–hole separation for solar-driven mesoporous rutile/anatase TiO <sub>2</sub> microsphere photocatalysts. RSC Advances, 2019, 9, 7870-7877.	3.6	18
66	Fabrication of Riceâ€Like Porous Anatase TiO <sub>2</sub> with High Thermal Stability and Enhanced Photocatalytic Performance. ChemCatChem, 2012, 4, 844-850.	3.7	17
67	Single-crystalline Bi <sub>19</sub> Br <sub>3</sub> S <sub>27</sub> nanorods with an efficiently improved photocatalytic activity. CrystEngComm, 2015, 17, 6120-6126.	2.6	17
68	Self‣upported NiS Nanoparticle oupled Ni <sub>2</sub> P Nanoflake Array Architecture: An Advanced Catalyst for Electrochemical Hydrogen Evolution. ChemElectroChem, 2017, 4, 1341-1348.	3.4	17
69	Achieving cadmium selenide-decorated zinc ferrite@titanium dioxide hollow core/shell nanospheres with improved light trapping and charge generation for photocatalytic hydrogen generation. Journal of Colloid and Interface Science, 2020, 575, 158-167.	9.4	16
70	Improved charge separation and carbon dioxide photoreduction performance of surface oxygen vacancy-enriched zinc ferrite@titanium dioxide hollow nanospheres with spatially separated cocatalysts. Journal of Colloid and Interface Science, 2021, 599, 1-11.	9.4	15
71	Fabrication of noncovalently functionalized brick-like β-cyclodextrins/graphene composite dispersions with favorable stability. RSC Advances, 2014, 4, 2813-2819.	3.6	14
72	Surface-oxygen vacancy defect-promoted electron-hole separation of defective tungsten trioxide ultrathin nanosheets and their enhanced solar-driven photocatalytic performance. Journal of Colloid and Interface Science, 2019, 557, 18-27.	9.4	14

#	Article	IF	CITATIONS
73	Sandwich-Structured Hybrid of NiCo Nanoparticles-Embedded Carbon Nanotubes Grafted on C <sub>3</sub> N <sub>4</sub> Nanosheets for Efficient Photodehydrogenative Coupling Reactions. ACS Applied Materials & Interfaces, 2022, 14, 24425-24434.	8.0	14
74	Confinement Effect on Ag Clusters in the Channels of Wellâ€Ordered Mesoporous TiO <sub>2</sub> and their Enhanced Photocatalytic Performance. ChemCatChem, 2013, 5, 1354-1358.	3.7	13
75	Efficient charge transfer and CO2 photoreduction of hierarchical CeO2@SnS2 heterostructured hollow spheres with spatially separated active sites. Applied Surface Science, 2022, 592, 153192.	6.1	13
76	Dyeâ€Sensitised Solar Cells Based on Largeâ€Pore Mesoporous TiO <sub>2</sub> with Controllable Pore Diameters. European Journal of Inorganic Chemistry, 2011, 2011, 4730-4737.	2.0	12
77	In situ intercalation and exploitation of Co3O4 nanoparticles grown on carbon nitride nanosheets for highly efficient degradation of methylene blue. Dalton Transactions, 2020, 49, 14665-14672.	3.3	12
78	Cu2O decorated α-Fe2O3/SnS2 core/shell heterostructured nanoarray photoanodes for water splitting. Solar Energy, 2021, 220, 843-851.	6.1	12
79	Efficient Separation of Photogenerated Charges in Sandwiched Bi <sub>2</sub> S <sub>3</sub> â^'BiOCl Nanoarrays/BiVO <sub>4</sub> Nanosheets Composites for Enhanced Photocatalytic Activity. ChemCatChem, 2020, 12, 3223-3229.	3.7	5
80	Efficient charge transfer in cadmium sulfide quantum dot-decorated hierarchical zinc sulfide-coated tin disulfide cages for carbon dioxide photoreduction. Journal of Colloid and Interface Science, 2022, 615, 606-616.	9.4	5